Proceedings of the 28th IEEE
EMBS Annual International Conference
New York City, USA, Aug 30-Sept 3, 2006

Segmentation of Prostate from 3-D Ultrasound Volumes Using Shape and Intensity Priors in Level Set Framework

Fuxing Yang, Jasjit Suri and Aaron Fenster

Abstract— **This paper presents a fully automatic prostate segmentation system in transrectal ultrasound images based on 3-D shape and intensity priors. 2-D manual segmentations from training image data are stacked to create the coarse 3-D shape. Min/Max flow is used to transform each coarse shape into smooth 3-D surface. Principle component analysis method is utilized to extract the 3-D shape mode from the training data sets. In a Bayesian inference, the nonlinear shape model is integrated with a nonparametric intensity prior and define a region based energy function. The energy is minimized in a level set frameworks and the control parameters of the convergence lead to the final segmentation. The developed method was tested on 3-D transrectal ultrasound images and its performance compared with manually-defined ground truth. The correct segmentation rate is 0.82.**

I. INTRODUCTION

Prostate cancer is the most commonly diagnosed malignancy in the group of men over the age of 50 [1]. It is the second leading cause of death due to cancer in men worldwide [2]. Ultrasound is a widely used imaging modality for prostate biopsy. The accurate detection of the prostate boundary in ultrasound images is of great importance for volume measurement and disease monitoring. However, in ultrasound images, the contrast is usually low and missing or diffuse boundaries is a very challenging problem for accurate segmentation of the prostate from the background.

Currently, many methods have been introduced to facilitate more accurate segmentation of the prostate boundaries from the ultrasound images. A large group of methods are based on edge information. Aarnink *et al.* [3] proposed a method for determination of the contour of the prostate in ultrasound images via an edge detection technique based on nonlinear Laplace filtering. The authors combined the information about edge location and strength to construct an edge intensity image. Then edges representing a boundary are selected and linked to build the final outline. Abolmaesumi *et al.* [4] used a Sticks filter to reduce the speckle and the problem is then discretized by projecting equispaced radii from an arbitrary seed point inside the prostate cavity towards its boundary. Candidate edge points obtained along each radius include the measurement points and some false returns. Pathak *et al.* [5], proposed an algorithm for guided edge delineation, which provided automatic prostate edge detection as a visual guide to the user. The edge detection contained contrast enhancement and anisotropic diffusion filter for smoothing image. However, the method needed a manual linking procedure on the detected edges.

Another group of methods need human interactivity as initialization. For example, Ladak *et al.* [6] proposed an algorithm, which used model-based initialization and a discrete dynamic contour. The user selected four points around the prostate. Then the outline of the prostate is estimated using cubic interpolation functions and shape information and the estimated contour is deformed automatically to better fit the prostate. Wang *et al.* [7] used a similar 2-D method. However, the authors segmented the remaining slices by iteratively propagating the result to the other slices and implementing the refinement. Hu *et al.* [8] used a model-based initialization and mesh refinement using deformable models. Six points were required to initialize the outline of the prostate using shape information. The initial outline was then automatically deformed to better fit the prostate boundary. Chiu *et al.* [9] introduced an algorithm based on the dyadic wavelet transform and the discrete dynamic contours. A spline interpolation was used to determine the initial contour based on four user-defined initial points. Then the discrete dynamic contour refined the initial contour based on the approximate coefficients and the wavelet coefficients generated using the dyadic wavelet transform. Ghanei *et al.* [10] proposed a three-dimensional deformable surface model for prostate segmentation based on a discrete structure, which was made from a set of vertices in the 3-D space as triangle facets. But this model also needed manual initialization from a few polygons drawn on different slices.

Pattern recognition based methods have also been widely used. Richard *et al.* [11] presented an texture-based algorithm, which segments a set of parallel 2-D images of the prostate into prostate and non-prostate regions. The algorithm utilizes a pixel classifier based on four texture energy measures associated with each pixel in the image. Clustering techniques are used to label each pixel in the image with the label of the most probable class. Prater *et al.* [12] use feed-forward neural networks for segmentation of the prostate in transrectal ultrasound images. These networks are trained using a small portion of a training image segmented by an expert and then applied to the entire training image.

Due to the weak boundary information, some researchers exploit statistical shape knowledge to help more accurate segmentation. Shen *et al.* [13] introduced a statistical shape

Fuxing Yang, PhD, is with Diagnostic Ultrasound 21222 30th Drive SE, Suite 120, Bothell, WA, 98021, USA. fuxing.yang@gmail.com

Jasjit Suri, PhD, FAIMBE, is with Biomedical Technologies Inc., Denver, CO, USA and also with Biomedical Research Institute (BRI), Idaho State University, ID, USA jsuri0256@msn.com

Aaron Fenster, PhD, FCCPM, is the Director and Scientist, at Imaging Research Laboratories, Robarts Research Institute. He is also the Professor of Medical Biophysics, Diagnostic Radiology and Nuclear Medicine, and Engineering at The University of Western Ontario, 100 Perth Drive, P.O. Box 5015, Canada afenster@imaging.robarts.ca

model to segment the prostate in transrectal ultrasound images. The authors used a Gabor filter bank in both multiple scales and multiple orientations to characterize the prostate boundaries. Then, a hierarchical deformation strategy was used. The model focused on the similarity of different Gabor features at different deformation stages using a multiresolution technique. Although the approach reached very high segmentation accuracy, the complexity and the computational cost were big barriers. Gong *et al.* [14] presented an approach based on deformable superellipses. Model initialization and constraining model evolution were based on prior knowledge about the prostate shape.

Generally in ultrasound images, prostate segmentation methods based on edge information have limitations when the image contains shadows with similar gray level and texture as the prostate region, or missing boundary segments. The similar pattern inside and outside the prostate brings more difficulties for the pattern recognition based method. Algorithms based on active contours have to depend on user interaction to determine the seed points. Although statistic shape information has been successfully applied, the convergence criterion based on the edge information makes the approach a non-robust solution.

In recent years, region based active contour techniques [15], [16], [17], [18] have been widely used in medical image analysis. The method can detect contours both with or without gradient, for instance objects with very smooth boundaries or even with discontinuous boundaries. The model has a level set formulation with a simple solution. The initialization of the contour also becomes simpler because the energy function defined by the shape and intensity prior, extracted from the training data set, will drive the contour to the location close to the object. Compared with edge based methods, this approach is robust and does not need extra human intervention. In this paper, we design and implement a system for fully automated 3-D prostate segmentation from transrectal ultrasound images, which uses shape and intensity knowledge in a level set framework.

II. Method

The method in our image analysis system includes three important steps: Shape prior extraction, intensity prior extraction and segmentation. Each step will be described in detail in the following subsections.

A. 3-D Shape Prior Extraction

A set of binary 3-D images $\{B_1, B_2, ..., B_n\}$, each of which is with 1 as object and 0 as the background. In order to extract the accurate shape information, alignment has to be applied. Alignment is a task to calculate the pose parameter p, which includes translation in x, y and z directions, rotation around x, y and z axis and scale in x, y and z directions.

The strategy to compute the pose parameters for n binary images is to use gradient descent method to minimize the special designed energy functional E^j_{align} for each binary image corresponding to the fixed one, say the first binary image B_1. The energy is defined as the following equation:

$$E^j_{align} = \frac{\int\int_\Omega (\tilde{B}_j - B_1)^2 dA}{\int\int_\Omega (\tilde{B}_j + B_1)^2 dA} \quad (1)$$

where Ω denotes the image domain, $\tilde{B}_j$ denotes the transformed image of B_j based on the pose parameters p. Minimizing this energy is equivalent to minimizing the difference between current binary image B_1 and the fixed image in the training database. The normalization term in the denominator is employed to prevent the images from shrinking to improve the cost function. Hill climbing or Rprop [19] method could be applied for the gradient decent.

The 3-D binary shape is from manual segmentation in each 2-D slice. The first step towards the 3-D shape model creation is to stack the 2-D segmentation. However, the stacked version is with a zigzagged surface and the accuracy is not guaranteed. We apply the Min/Max flow [20] method to smooth the 3-D surface and increase the accuracy between every 2 slices. Min/Max flow uses the curvature based force to fix the surface and the patch on the surface with large positive or small negative curvatures will be smoothed, which can not be done by simply creating meshes based on adjacent contours. In Fig. 1, one example is shown how the Min/Max flow could smooth the 3-D surface.

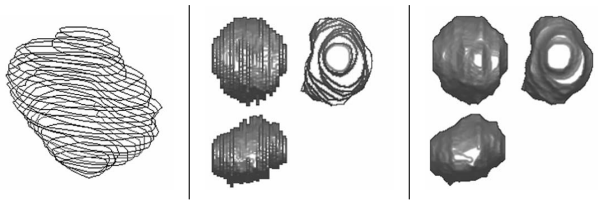

Fig. 1. Using Min/Max flow to smooth 3-D surface. The image on the left is the 2-D contours from manual tracing in 3-D space. The image in the middle is the 3 views of the surface rendering of the 3-D shape from stacked 2-D manual segmentation. On the right is the 3 views and surface rendering of the 3-D surface after Min/Max flow.

After using Min/Max flow method for each 3-D surface, we collected a set of 3-D training shapes encoded by their signed distance functions. Tsai *et al.* [15] proposed an efficient method to reduce the segmentation problem to one of finite-dimensional optimization by constraining the optimization problem to the finite-dimensional subspace spanned by the training shapes. Then a new level set function is defined to represent the 3-D shape as:

$$\Phi[w] = \bar{\Phi} + \sum_{i=1}^{k} w_i \Phi_i \quad (2)$$

where $w = \{w_1, w_2, ..., w_k\}$ are the weights for the k eigenshapes. Now we can use this newly constructed level set function Φ as the implicit representation of shape. Specifically, the zero level set of Φ describes the shape with the shapes variability directly linked to the variability of the level set function. Therefore, by varying w, Φ will be changed, which indirectly varies the shape. The average shape and several shape variances are illustrated in Fig. 2.

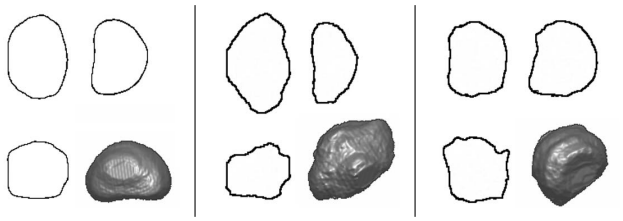

Fig. 2. 3 views and surface rendering of the mean shape is in the first image. The image in the middle is the mean shape + 1st eigenshape. On the right is the mean shape - 1st eigenshape.

B. Intensity Prior Extraction

Although for certain imaging modalities such as ultrasound or CT, the structures of interest do not differ much from their background, the intensity information in the image can be utilized by probabilistic intensity models. From the training data set, we classify the image as foreground and background. The corresponding histograms provide the conditional probability for different gray level inside and outside the segmentation. This information can be efficiently combined with the shape prior for final segmentation. [Fig. 3]

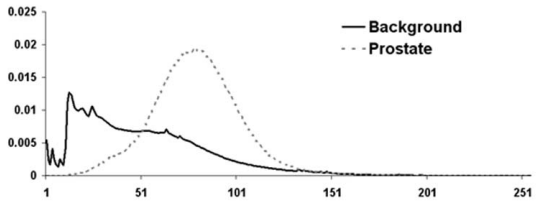

Fig. 3. In this prostate segmentation project, we have the two intensity distributions corresponding to the empirical probability of intensities inside and outside the prostate.

C. Segmentation as Bayesian Interface

Segmentation in the level set framework can be formulated as the estimation of the optimal embedding function $\Phi : \Omega \rightarrow \Re$ given an image $I : \Omega \rightarrow \Re$ [16]. In the Bayesian framework, this can be computed by maximizing the posterior distribution

$$P(\phi|I) \propto P(I|\phi)P(\phi) \tag{3}$$

Based on the result from equation (2), the Bayesian interface problem stated in equation (3) can be solved in a problem as the following conditional probability

$$P(w,p|I) \propto P(I|w,p)P(w,p) \tag{4}$$

is optimized with respect to the weight w and the pose parameter p. Maximization of the posterior probability or equivalently minimization of its negative logarithm is able to create the most probable segmentation of a given image. Combined with the shape and intensity priors we collected from the previous two sections, a new energy can be defined as

$$E(w,p) = -\log P(I|w,p) - \log P(w,p) \tag{5}$$

We choose the method introduced in [16] to compute the energy and refer to that paper for more details. The energy function is a variation from the Mumford-Shah function which has been utilized in medical image processing [15]. The minimization of the energy function can be made through gradient descent method like Rprop [19].

III. Experiment Methods

A. Transrectal Ultrasound Images

The 3-D TRUS images were obtained from the Imaging Research Laboratories of the Robarts Research Institute, using an Aloka 2000 US machine (Aloka, CN) with a biplane side-firing TRUS transducer mounted on a motorized scanning mechanism. The transducer rotated about its axis through a scanning angle, while a series of 120 2-D B mode images were acquired with an 8-bit video frame grabber at 15Hz. For each 3-D scan, the acquired 2-D images were reconstructed into a 3-D image, using reconstruction software developed in the laboratory, with the z-axis parallel to the transducer axis. The sizes of the images are 860 by 427 by 348 and the voxel size is 0.154 by 0.154 by 0.154 mm^3.

B. Validation Method

11 manually extracted prostates were collected from 11 different patients. We employed a jackknifing strategy by removing the image of interest from the training phase.

We used the outlines from manual tracing as an independent standard, which was done by an experienced radiologist. In section II-A, we have collected the 3-D close surface using the 2-D manual tracing and used these smoothed 3-D surfaces as the final ground truth.

The validation indices are defined as the following two parameters: correct segmentation rate(CSR) and incorrect segmentation rate (ISR). CSR is defined as the ratio of correct segmentation voxel number and the total voxel number of the ground truth. ISR is defined as the ratio of the incorrect (the non-prostate voxel is classified as prostate voxel) segmentation voxel number and the total voxel number of the ground truth.

IV. Results

Our segmentation method successfully determined the prostate in all 11 ultrasound images. As we introduced in the previous section, we used the jackknifing method for validation. For every ultrasound image, we use the remaining 10 to extract the shape and intensity priors. Using the computed shape model and intensity knowledge, we initialized the mean shape at the center of the image and started the gradient decent method to find the best pose parameters and weight factors. On average, correct segmentation rate (CSR) was 0.82 and the incorrect segmentation rate (ISR) was 0.19. Also, the standard deviation of the CSR and ISR correspondingly were 0.05 and 0.08. Fig. 4 shows coronal and axial view of 2 results overlapped on the original images.

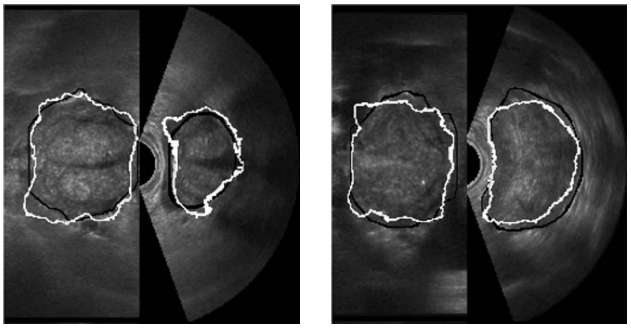

Fig. 4. Coronal and axial views of the prostate segmentation (white) from 2 different patients and the overlaid manual segmentation (black).

V. CONCLUSIONS AND FUTURE WORKS

A. Conclusions

The segmentation of prostate from ultrasound images is an important and challenging problem. In the context of ultrasound imagery, the main challenges include: the edge information of the objects is too weak; speckle noise degrades the images. Existing algorithms that use edge information depend on extra image enhancement methods and even need user interaction for initialization or editing.

In this paper, we reported a system, which incorporates learned shape models and intensity prior for the objects of interest using level set methods. The algorithm allows the shape to evolve until the optimal segmentation is found by minimizing a region based energy factor without special initialization. The quantitative analysis proved that the method is a robust solution for fully automated prostate segmentation task in ultrasound image.

B. Future Works

In this work, the quantitative analysis of the method is based on a small number of image data and the corresponding ground truth. It is possible that the shape model and intensity prior extracted from the limited training data is not able to deal with more complicated situations. As we will acquire more data sets, we believe the segmentation accuracy based on a larger number of training data will be increased. Also, the 2D manual tracing for training was not created at every slice from the original ultrasound image. Although we employed the Min/Max flow method to make a smooth interpolation, the resulting 3-D surface was still not accurate enough. Adding manual tracing in more slices will be a solution.

Although there are many advantages using the above methods in a level set framework, as a fully automated 3-D approach, the computational cost is still a big barrier. In this paper, we exploited the kernel density estimation [16] to increase the efficiency. The total convergence time is still over 70 seconds. (The hardware environment is PC with Pentium(R) 4 CPU 2.80GHz and 1.00GB of RAM) Optimization work will be done in the future to make the method more practical for prostate segmentation from ultrasound images.

We provide a 3-D validation result in this paper. However, comparison needs to be done between our method and other methods, including segmentation accuracy and computational and memory cost.

REFERENCES

[1] L. Garfinkel and M. Mushinski, "Cancer incidence, mortality, and survival trends in four leading sites," *Stat. Bull. Metrop. Insur. Co.*, vol. 75, pp. 19–27, 1994.

[2] E. Silverberg, C. C. Boring, and T. S. Squires, "Cancer statistics," *CA Cancer J. Clin*, vol. 40, pp. 9–26, 1990.

[3] R. Aarnink, A. Huynen, J. Rosette, F. Debruyne, and H. Wijkstra, "A practical clinical method for contour determination in ultrasonographic prostate images," *Ultrasound in Medicine and Biology*, vol. 20, pp. 705–717, 1994.

[4] P. Abolmaesumi and M. Sirouspour, "Segmentation of prostate contours from ultrasound images," in *Proceedings of IEEE International Conference on Acoustics, Speech and Signal Processing*, vol. 3, 2004, pp. 517–520.

[5] S. Pathak, V. Chalana, D. Haynor, and Y. Kim, "Edge-guided boundary delineation in prostate ultrasound images," *IEEE Transactions on Medical Imaging*, vol. 19, pp. 1211–1219, 2000.

[6] H. Ladak, F. Mao, Y. Wang, D. Downey, D. Steinman, and A. Fenster, "Prostate boundary segmentation from 2d ultrasound images," *Medical Physics*, vol. 27, pp. 1777–1788, 2000.

[7] Y. Wang, H. Cardinal, D. Downey, and A. Fenster, "Semiautomatic three-dimensional segmentation of the prostate using twodimensional ultrasound images," *Medical physics*, vol. 30, pp. 887–897, Sep 2003.

[8] N. Hu, D. Downey, A. Fenster, and H. Ladak, "Prostate boundary segmentation from 3d ultrasound images," *Medical Physics*, vol. 30, pp. 1648–1659, 2003.

[9] B. Chiu, G. Freeman, M. Salama, and A. Fenster, "Prostate segmentation algorithm using dyadic wavelet transform and discrete dynamic contour," *Phys Med Biol*, vol. 49, pp. 4943–4960, 2004.

[10] A. Ghanei, H. Soltanian-Zadeh, A. Ratkesicz, and F. Yin, "A three-dimensional deformable model for segmentation of human prostate from ultrasound image," *Medical Physics*, vol. 28, pp. 2147–2153, 2001.

[11] W. Richard and C. Keen, "Automated texture-based segmentation of ultrasound images of the prostate," *Computerized Medical Imaging and Graphics*, vol. 20, pp. 131–140, 1996.

[12] Prater, J.S., and W. Richard, "Segmenting ultrasound images of the prostrate using neural networks," *Ultrasound Imaging*, vol. 14, pp. 159–185, 1992.

[13] D. Shen, Y. Zhan, and C. Davatzikos, "Segmentation of Prostate Boundaries From Ultrasound Images Using Statistical Shape Model," *IEEE Transactions on Medical Imaging*, vol. 22, no. 4, pp. 539–551, 2003.

[14] L. Gong, S. Pathak, D. Haynor, P. Cho, and Y. Kim, "Parametric Shape Modeling Using Deformable Superellipses for Prostate Segmentation," *Medical Physics*, vol. 23, pp. 340–349, 2004.

[15] A. Tsai, A. Yezzi, W. Wells, C. Tempany, D. Tucker, A. Fan, W. E. Grimson, and A. Willsky, "A shape-based approach to the segmentation of medical imagery using level sets," *IEEE Transactions on Medical Imaging*, vol. 22, pp. 137–154, 2003.

[16] M. Rousson and D. Cremers, "Efficient kernel density estimation of shape and intensity priors for level set segmentation," in *Proceeding of International Conference on Medical Image Computing and Computer Assisted Intervention (MICCAI)*, vol. 1, 2005, pp. 757–764.

[17] F. Yang, J. S. Suri, and M. Sonka, "Volume segmentation using active shape models in level set framework," in *Parametric and Geometric Deformable Models: An application in Biomaterials and Medical Imagery*, J. S. Suri and A. Farag, Eds. Springer, May 2006.

[18] J. S. Suri, D. L. Wilson, and S. Laxminarayan, *Hand Book of Medical Image Analysis*. Springer, 2006.

[19] M. Riedmiller and H. Braun, "A direct adaptive method for faster backpropa-gation learning: The rprop algorithm," in *Proceeding of the IEEE International Conference on Neural Networks*, 1993, pp. 586–591.

[20] R. Malladi and J. A. Sethian, "Image Processing via Level Set Curvature Flow," in *Proceedings of the National Academy of Sciences*, vol. 92, Jul 1995, pp. 7046–7050.